Intermolecular Interactions of IgG1 Monoclonal Antibodies at High Concentrations Characterized by Light Scattering

Thomas M. Scherer,* Jun Liu, and Steven J. Shire

Genentech Incorporated, Late Stage Pharmaceutical and Processing Development, 1 DNA Way, South San Francisco, California 94080

Allen P. Minton

Laboratory of Biochemistry and Genetics, National Institute of Diabetes, Digestive, and Kidney Diseases, National Institutes of Health, U.S. Department of Health and Human Services, Bethesda, Maryland 20892

Received: March 30, 2010; Revised Manuscript Received: July 16, 2010

Light scattering intensity measurements of solutions of two purified monoclonal antibodies were performed over a wide range of concentrations (0.5−275 mg/mL) and ionic strengths (0.02 to 0.6 M). Despite extensive sequence homology between these mAbs, alteration of ∼20 amino acids in the complementarity determining regions resulted in different net intermolecular interactions and responses to solution ionic strength. The concentration dependence of scattering was analyzed by comparison with the predictions of three models, allowing for intermolecular interaction of various types. In order of increasing complexity, the three models account for: (1) steric repulsions (simple hard-sphere model), (2) steric repulsion with short-ranged attractive interactions of varying magnitude (adhesive hard-sphere model), and (3) steric and nonsteric repulsive interactions between several species whose relative concentrations may change as a function of total protein concentration as dictated by equilibrium self-association (effective hard-sphere mixture model). Simple scattering models of noninteracting and adhesive hard-sphere species permitted qualitative interpretation of contributions from excluded volume, electrostatic, and van der Waals interactions on net mAb interactions at high concentration as a function of ionic strength. mAb2 electrostatic interactions were repulsive, whereas mAb1 interactions were net attractive at low ionic strengths, attributed to an anisotropic distribution of molecular charge. The effective hard-sphere mixture model can account quantitatively for the dependence of scattering for both antibodies over the entire concentration range and at salt concentrations exceeding 40 mM. This analysis showed that at high ionic strength both mAbs self-associate weakly to form dimer with an affinity that varies little with salt concentration at concentrations exceeding 75 mM. In addition, mAb1 appears to self-associate further to form oligomers with stoichiometry of 4−6 and an affinity that declines substantially with increasing ionic strength. All three models lead to the conclusion that at high concentrations repulsive interactions are predominantly due to excluded volume, whereas additional features are salt-dependent and reflect a substantial electrostatic contribution to intermolecular interactions of both mAbs.

Introduction

The frontiers of investigating protein−protein interactions are currently at the upper and lower boundaries of measurable protein concentration. Recent work demonstrates that with extremely limited sample quantities, protein−protein interactions in solution can be measured in microfluidic devices with back scattering interference down to nanomolar concentrations.[1] Other similar techniques such as surface plasmon resonance (SPR), quartz microbalance, and fluorescence resonance energy transfer (FRET) methods have been developed into powerful tools for investigating generally strong, specific lock and key binding or affinity interactions to tease apart the complex biological roles proteins have when interacting with one another in living organisms.[2] Interactions between proteins in highly dilute solutions, however, do not reflect the full range of intermolecular interactions experienced in vivo, where concentrations of proteins and other macromolecules can be as high as 300−500 mg/mL.[3] Therefore, the investigation of protein interactions and association at very high concentrations will also contribute important knowledge of complex interactions in biological systems and concentrated colloidal solutions.

Protein intermolecular interactions examined at high concentrations are not limited to strong or specific molecular binding interactions but also frequently include weak, long-range as well as short-range nonspecific interactions that are the result of molecular, chemical, and interfacial properties of the protein's constituent atoms and surfaces. An early endeavor in the field of biophysics, the study of proteins at high concentrations was initially conducted with a limited set of proteins that were available in large quantities from animal sources: hemoglobin,[4] serum albumin,[5] and eye lens crystallins.[6] The techniques first applied to the investigation of high concentration systems included osmotic pressure,[4,7] sedimentation equilibrium,[8,9] viscometry,[10] and light scattering.[11,12] More recently, investigations into the interactions of high concentration protein solutions have also employed NMR methods,[13,14] tracer sedimentation equilibrium,[15] high-frequency quartz crystal rheology,[16] and light scattering methods. Scattering techniques including static light scattering (SLS), dynamic light scattering (DLS), small-angle

* Corresponding author. Tel: (650) 467-3338. Fax (650) 225-3613. E-mail: tscherer@gene.com.

10.1021/jp1028646
Published on Web 09/17/2010

X-ray scattering (SAXS), and small-angle neutron scattering (SANS) have demonstrated their utility in the study of high concentration systems.[17−20] These scattering methods remain among the most versatile tools for examining protein interactions and structure in solution.

Interpreting the results from the above methods without exception still presents a challenge because most underlying analytical theories are based on ideal, dilute solution measurement conditions. Proteins in high concentration solutions cannot be treated as isolated, noninteracting species. Early theories for interpretation of nonideal behavior in highly concentrated protein solutions utilized hard-sphere models together with various equations of state[10] to account for the excluded volume effect or "molecular crowding" where particles are mutually excluded from occupying the same space. (For review, see ref 21.) For interacting particles, where the model consists of a single species of adhesive hard spheres (AHSs), an analytical solution for the equation of state was explicitly derived.[22] This has enabled description of solution nonideality of hard particles of known size with variable strength short-range attractive interactions. Physically, the AHS model provides an approximation of the role played by van der Waals and other short-range forces in protein−protein interactions.[23,24] This model successfully described concentration-dependent light scattering by lysozyme[25] and γ-crystallin[19] solutions as a function of temperature and moderate (0.1 to 0.2 M) salt concentrations. A more explicit molecular thermodynamic model incorporated two-Yukawa potentials to describe the concentration dependence of osmotic pressure in BSA, lysozyme, α-chymotrypsin, and IgG solutions with salts from 0.1 to 5.0 M.[26] The success of these models provides an understanding of systems in which nonspecific attractive protein−protein interactions are effective over very short distances relative to the size of the molecule in solution. However, Baxter AHS and molecular thermodynamic approaches were found to be less effective in describing systems with high ionic strength or strong association/attractive interactions.

SANS and SAXS can be used to measure solution structure factors over a broad range of protein concentrations, which may be modeled with effective pair-interaction potentials that typically include contributions from repulsive electrostatic and excluded volume interactions and attractive van der Waals forces to provide details of protein interactions as a function of distance.[27,28] SAXS structure factors have been obtained for α- and γ-crystallins,[29] lysozyme,[30] hemoglobin,[31] cytochrome c,[32] and BSA.[33] Simulations of the structure factors successfully described systems in which net interactions are repulsive, modulated with either molecular net charge or the strength of the repulsive force, but were also found to have significant limitations when describing systems where attractive interactions dominate.[30,33]

Recently, the calculation of total scattering due to the presence of multiple species of scatterers in chemical equilibrium with each other using an effective hard particle model was developed by Minton.[34] This model addresses contributions from strong attractive interactions to form additional scattering species. According to this model, macromolecular species are represented by an equivalent hard convex particle with the mass of the macromolecule and size, parametrized by a specific exclusion volume that reflects both the hard steric core and short-ranged repulsive interactions with neighboring molecules. It has been demonstrated that the effective hard-sphere model can account quantitatively for the concentration dependence of experimentally measured SLS of solutions of individual non-self-associating proteins,[11,35] binary mixtures of nonassociating proteins, and a self-associating protein[36] over a broad range of concentrations with a minimum of adjustable parameters. The specific exclusion volume may vary with experimental conditions because it reflects not only hard core steric repulsion but also "soft" repulsive intermolecular interactions, and depending on the mechanism of interaction, it may vary with pH, temperature, or ionic strength.[34,37]

We investigated the solution scattering of monoclonal antibodies (mAbs) with the specific aim of understanding the differences in mAb self-interactions in highly concentrated solutions. Significant deviations from ideal solution properties at high protein concentrations can pose substantial challenges during therapeutic product development, manufacture, and administration to the patient.[38] In this work, SLS was used to characterize the molecular interactions of two IgG1 mAbs at high concentrations, obtaining Rayleigh scattering $R(\theta,w)$ intensity as a function of protein concentration and solution ionic strength. Models based on single scattering species of hard spheres as well as models that consider thermodynamic equilibrium contributions of multiple species of scatterers were used to interpret the data over the continuum of concentrations for two similar mAbs in solutions of varying ionic strength. The results present evidence of the diversity and complexity of intermolecular protein interactions at high concentrations.

Experimental Methods

mAb1 and mAb12 are humanized mAbs based on the same IgG1 framework and κ-light chains, with approximately 20 amino acid residue differences located in the complementarily determining regions (CDRs). These antibodies were expressed in Chinese hamster ovarian (CHO) cell lines and purified by a series of chromatography steps, including protein A and ion exchange chromatography methods. The purified antibodies were obtained as concentrated solutions from tangential flow filtration with added solution buffers and stabilizers, with mAb1 at 196 mg/mL and mAb2 at 166 mg/mL. mAb1 and mAb2, the molecules used in the present study, are the same IgG_1 molecules referred to in previous studies by Liu et al.,[39] Kanai et al.,[40] and Yadav et al.[41]

These stock mAb starting materials were stored at 2−8 °C until further use. Additional preparation of mAb solutions included dialysis using Spectrapore 6−8 kD MWCO membrane (Spectrum Laboratories, CA). Approximately 50−60 mL stock solutions were dialyzed against 1.2 L of low ionic strength buffer containing 10 or 30 mM histidine−HCl at pH 6.0 over 48 h at 2−8 °C for a minimum of three buffer exchanges. The dialyzed mAb solutions were filtered through 0.22 μm modified PVDF filters (Millipore Steriflip, Millipore, MA) to remove large particulates. Typically, mAb concentrations of 140−150 mg/mL were obtained after dialysis. mAb1 and mAb2 antibody preparations consisted of >98% monomer, as determined by size exclusion chromatrography analysis of samples diluted to 1 mg/mL. To obtain the higher mAb concentrations, 10 mL of mAb dialyzed in 30 mM histidine−HCl, pH 6.0 was concentrated with Amicon YM30 Centriprep (Millipore, MA) concentrators centrifuged at 2700 rpm (1500 G) with removal of filtrate at 3 h intervals until the desired concentration was obtained. We determined final mAb concentrations in the dialyzed and centrifugally concentrated preparations by using gravimetric dilutions and absorptivities at 280 nm (A_{280}) of 1.6 and 1.5 (mg/mL) cm^{-1} for mAb1 and mAb2, respectively, and measurement of UV absorption at 280 nm using an Agilent diode array spectrophotometer model 8453 with a 1 cm path length quartz

cuvette. Extinction coefficients were determined by quantitative amino acid analysis. Deionized water from a Milli-Q Biocel purification system with 0.22 μm filter was used for all aqueous solution preparations. All buffers and reagents were analytical grade or higher purity. All buffer solutions were titrated to the correct pH and filtered using Millipore Stericup GV 0.22 μm filters.

mAb solutions for light scattering experiments were prepared in 20 mL scintillation vials over 0.5 to 295 mg/mL by gravimetric dilution of known stock solution concentrations in a laminar flow hood. All scintillation vials were carefully cleaned with deionized water and dried in a stream of filtered compressed nitrogen gas. Before addition to protein solutions, all buffer and reagent solutions were additionally filtered through 0.10 μm Whatman Anotop 25 filters. Sodium chloride was introduced to the samples as a 0.1 μm filtered 4.0 M solution with gravimetric measurement of initial and final mass, with volumes adjusted to achieve the desired NaCl concentration in each vial. After preparation or dilution of the samples, mAb solutions were mixed to homogeneity and allowed to reach thermal and chemical equilibrium at controlled room temperature for 2 h. Protein solutions were centrifuged at room temperature for 20−30 min at 3000 rpm to remove adventitious dust and bubbles from the solutions prior to use for light scattering. The most concentrated solutions (mAb > 170 mg/mL) were centrifuged for greater lengths of time until the light scattering signal showed a minimum of noise. Exterior surfaces of scintillation vials were lightly coated with silicone oil to reduce undesired scattering from vial surface defects. Samples prepared as above were directly placed in the light scattering instrument for measurements.

Static Light Scattering from Solutions of a Single Species. For a single scattering species at arbitrary concentration, the Rayleigh ratio ($R(\theta,w)$) is given by eq 1.[42] In this limiting case, which can be applied to systems of monodisperse molecules (e.g., many purified proteins), $R(\theta,w)$ is a function of the scattering angle θ and w/v concentration w and is directly related to the mass of the scattering species (M), the molecular size and shape through the form factor $P(\theta)$, and interactions between scatterers described by the structure factor $S(\theta,w)$

$$R(\theta, w) = KwMP(\theta)S(\theta, w) \tag{1}$$

where

$$K = \frac{4\pi^2 n^2}{N_A \lambda_o^4}\left(\frac{dn}{dw}\right)^2$$

The optical constant K is a function of the solution refractive index (n),[43] the wavelength of incident light (λ_o), the specific refractive index increment of scattering solute (dn/dw), and Avogadro's number (N_A). In the limit of infinite dilution ($w \rightarrow 0$) and infinitesimal scattering angle ($\theta \rightarrow 0°$), eq 1 yields the value of M. In practice, light scattering measurements are made at both finite concentrations and angles, extrapolating to one or both limiting conditions to obtain M. Because many of the measurements discussed herein are far outside the approximation of infinite dilution, we introduce the value of apparent molecular mass (M_{wApp}), obtained at concentration w in the limit of $\theta \rightarrow 0°$, with the virial expansion terms (A_2, A_3, etc.) in the denominator of eq 2 accounting for the intermolecular interactions between identical scattering species.

$$\frac{R(0°, w)}{Kw} = M_{wApp} = M\left[\frac{1}{[1 + 2A_2Mw + 3A_3Mw^2...]}\right] \tag{2}$$

An 18-angle Dawn EOS light scattering detector with a 30 mW solid-state laser ($\lambda = 690$ nm) from Wyatt Technology (Santa Barbara, CA) was used for all SLS measurements with a water-cooled Peltier temperature controller set at 23 °C. The instrument was calibrated with 99.9% toluene (chromatography grade). For a typical scintillation vial experiment, a detector gain setting of 1× was used for all photodiodes at fixed angles from 38 to 148°. Because the radius of gyration (R_G) of mAb2 is less than 10 nm, a dilute solution (1 to 2 mg/mL) of mAb2 was used at each salt concentration to normalize the voltages of the photodiodes relative to the 90° detector using a photodiode detector gain setting of 21× at the end of each experiment. Measurement of SLS intensity was conducted as a function of mAb concentration from 0.5 mg/mL to 295 mg/mL and as a function of NaCl concentration (0−600 mM). Scattering data for each sample/vial was collected over an interval of 5−10 min with a data collection frequency of 12 points/minute. Astra 4.90.07 Software (Wyatt Technology Corporation, Santa Barbara, CA) was used to acquire and process the SLS data, with a dn/dw value of 0.185 mL/g applied to calculations that could be exported as slice results. Further analysis and calculations with the exported results were conducted in Microsoft Excel, Origin v7.5, and MATLAB R14.

Second Osmotic Virial Coefficient Measurement. Second osmotic virial coefficients (A_2) and the antibody molecular mass (M) were determined from samples <10 mg/mL (usually three to four concentrations) and linear extrapolation to infinite dilution. Uncertainties reported are from linear fitting error and do not represent A_2 measurement reproducibility. The osmotic second virial coefficients represent the net magnitude of the two-body interactions of a single species of scatterers.

Simulation of Static Light Scattering from Hard Spheres. Experimental results were compared with light scattering intensities calculated using Raleigh−Debye−Gans (RDG) scattering theory[44] and the Percus−Yevick approximation of the solid-sphere structure factor as outlined by Bettelheim and Siew.[45] In brief, in RDG theory, the intensity of unpolarized light scattered from a suspension containing volume fraction ϕ (described below) of hard spherical particles that are much smaller than the wavelength of incident light is given by

$$R(\theta, \varphi) = \frac{6\pi^3 n_2^4 r^3}{\lambda_0^4}\left(\frac{m^2 - 1}{m^2 + 2}\right)^2 (1 + \cos^2\theta)S(\theta, \varphi)P(\theta, 0)\varphi \tag{3}$$

where r is the radius of the spherical scatterer, λ_0 is the wavelength of incident light in vacuum, m is the ratio (n_1/n_2) of the refractive index of the scatterer (n_1) to the solution (n_2), $S(\theta,\varphi)$ denotes the structure factor, and $P(\theta)$ denotes the form factor. For the systems investigated here, $\lambda_o = 690$ nm, the refractive index $n_2 = 1.331$, and assuming that the refractive index difference between scatterer and diluent remains constant as in RDG theory, the refractive index term ($m^2 - 1/m^2 + 2$) is approximated as $2(dn/dw)/3n_2$. A dn/dw value of 0.185 mL/g was used for both mAbs.[46] Other simplifications of the equation above resulted from the use of monochromatic and plane polarized light so that the term $1 + \cos^2\theta$ becomes unity, and because the angular dependence of light scattered was very small

(IgG1 mAb radii of gyration are $<\lambda_o/20$), the form factor $P(\theta)$ could also be reduced to unity. It should be noted that the correct Percus−Yevick equation for the inverse structure factor $S(\theta,\varphi)^{-1}$ of a sphere was obtained elsewhere,[47] as shown below.

$$\frac{1}{S(\theta,\phi)} = 1 + \frac{24\varphi}{u^3} \times \left\{ \begin{array}{l} a(\sin u - u\cos u) + b\left[\left(\frac{2}{u^2} - 1\right)u\cos u + 2\sin u - \frac{2}{u}\right] + \\ \frac{\varphi a}{2}\left[\frac{24}{u^3} + 4\left(1 - \frac{6}{u^2}\right)\sin u - \left(1 - \frac{12}{u^2} + \frac{24}{u^4}\right)u\cos u\right] \end{array} \right\} \quad (4)$$

where r is the radius of the sphere, n_o is the solvent refractive index, and the terms are defined as follows

$$u = 2qr \quad q = \frac{4\pi n_o(\sin\theta/2)}{\lambda_o} \quad a = \frac{(1+2\varphi)^2}{(1-\varphi)^4} \quad b = -\frac{3}{2}\varphi\frac{(\varphi+2)^2}{(1-\varphi)^4}$$

Volume fractions (φ) can be obtained by selecting a value for a sphere-equivalent radius (r) and using the molecular weight (M) for mAb ≈ 150 kDa, where w is protein concentration in grams per milliliter and N_A is 6.022×10^{23} mol^{-1}

$$\varphi = \frac{4\pi r^3 N_A w}{3M} \quad (5)$$

We facilitated further comparison of results by using the experimental optical constant $K_o = 1.7504 \times 10^{-7}$ based on the refractive index of the solvent (constant, and distinguished from K, which incorporates the refractive index of the scattering solution and depends on mAb concentration) and calculation of the apparent M_w and osmotic compressibility plots of $Kc/R(\theta)$ versus concentration representative of a hard sphere with $dn/dw = 0.185$ mL/g.

Adhesive Hard-Sphere Model Calculations. Calculations of the scattering from AHS models were made according to the analytical solution to the P−Y approximation derived by Barboy[48] and presented in the limit of $\theta \to 0$ for $S(\theta,\varphi)^{-1}$ by Fine et al.[19]

$$\frac{1}{S(\theta,\varphi)} = \frac{[1 + 2\varphi - \xi\varphi(1-\varphi)]^2}{(1-\varphi)^4} \quad (6)$$

$$\xi = 6\left(\frac{\tau}{\varphi} + \frac{1}{1-\varphi}\right) - \sqrt{\left[6\left(\frac{\tau}{\varphi} + \frac{1}{1-\varphi}\right)\right]^2 - \frac{12(1+\varphi/2)}{\varphi(1-\varphi)^2}} \quad (7)$$

The strength of the adhesive or attractive interactions can be modulated through τ, a dimensionless parameter that characterizes the interaction potential well depth. The approximate analytical solution for attractive interactions described above by τ (eq 7) is achieved in the limit of a potential with infinitesimally narrow width. To examine the results and limitations of this model, we use eqs 6 and 7 together with eqs 3 and 5 to calculate the dependence of R upon w for mAb with attractive intermolecular interactions over the range of τ values ($\infty > \tau > 0.1$). In the limit of $\tau = \infty$, the Baxter AHS model results reduce to the scattering from a simple hard sphere (eq 3).

Modeling of Macromolecular Solution Nonideality with Thermodynamic Expressions for Self-associating Hard Spheres. The noninteracting hard sphere and AHS models are applicable only to solutions containing a single species of scattering particles. An approach more generalized to mixtures of interacting species is provided by the thermodynamically based fluctuation theory of light scattering.[49,50] According to this theory, when all scattering species are small relative to the wavelength of incident light, the (angle-independent) scattering intensity of a mixture of species is given by

$$\frac{R(\theta)}{K} = \sum M_i M_j \langle \Delta c_i \Delta c_j \rangle \quad (8)$$

where M_i denotes the molecular weight of the ith scattering species, $\langle \Delta c_i \Delta c_j \rangle$ denotes the average fluctuation correlation of the molar concentrations of scattering species i and j, and K is identical to the optical constant defined in eq 1. Expressions for $\langle \Delta c_i \Delta c_i \rangle$ and $\langle \Delta c_i \Delta c_j \rangle$ as functions of species concentration c_i and the partial derivatives of thermodynamic activity coefficients with respect to molar concentration ($\partial \ln \gamma_i/\partial c_j$) in mixtures of up to three scattering species have been presented elsewhere.[51]

The total scattering of a mixture of a monomer and up to two oligomeric species (n-mer and m-mer) in equilibrium with monomer is calculated as follows. The equilibrium association constants (K_{1i}) are defined

$$K_{1i} = \frac{a_i}{a_1^i} = \frac{c_i}{c_1^i}\frac{\gamma_i}{\gamma_1^i} \quad (9)$$

where a_i and γ_i, respectively, denote the thermodynamic activity and activity coefficient of i-mer. Activity coefficients and the partial derivatives of activity coefficients with respect to species concentrations are calculated as a function of solution composition (c_1, c_n, and c_m) utilizing relations derived from the scaled particle theory of hard-sphere mixtures[52] together with an effective hard-sphere model, according to which each species is represented by a sphere with volume proportional to mass and a uniform effective specific volume (v_{exc}).[51] The concentrations of monomer, n-mer, and m-mer at equilibrium are obtained by numerical solution of the conservation of mass equation

$$c_{tot} = \frac{w_{tot}}{M_1} = c_1 + nc_n + mc_n = c_1 + nK_{1n}\frac{\gamma_1^n}{\gamma_n}c_1^n + mK_{1m}\frac{\gamma_1^m}{\gamma_m}c_1^m \quad (10)$$

Because species concentrations and activity coefficients are interdependent, eqs 9 and 10 and the equations specifying species activity coefficients as functions of c_1, c_n, and c_m must be solved numerically in an iterative fashion to convergence.[51] Once equilibrium values of the c_i and γ_i are obtained, the values of $\partial(\ln \gamma_i)/\partial c_j$, $\langle \Delta c_i \Delta c_j \rangle$ and subsequently $R(\theta)/K$ are calculated as described above.

The association state(s) of the oligomer species (n and m) are obtained from fitting a global model with monomer mass (M_1), and association constants K_{1n} and K_{1m} for each solution condition. The effective hard spherical model also employs an adjustable parameter v_{exc}, referred to as the effective

specific exclusion volume, which reduces to the actual partial specific volume in the absence of electrostatic repulsion (i.e., near the isoionic pH of the protein). More generally, v_{exc} exceeds the mAb partial specific volume to provide a measure of the repulsive intermolecular interactions in concentrated solution.[34] In the absence of self-association, this model reproduces the scattering obtained for a uniform fluid of hard spheres calculated using eqs 3 and 4.

The data obtained for all angles at any single concentration were averaged to obtain an angle-independent value of $<R(\theta)>/K_o$. Using scripts and functions written in MATLAB (R2007b, Mathworks, Natick, MA, available upon request from APM), nonlinear least-squares modeling of the measured scattering intensity dependence upon the concentration of all scattering species (w_{tot}) was carried out for each protein solution in which NaCl equaled or exceeded 40 mM NaCl. Data obtained at lower salt concentrations were not modeled because the effective hard particle model used is not expected to be realistic under low ionic strength conditions, where the range of electrostatic interactions is comparable to or exceeds the dimensions of the interacting molecules.[21]

Results and Discussion

Previous characterization of the solution of both monoclonal antibodies mAb1 and mAb2 showed surprising differences in solution behavior with small differences in the amino acid sequence. The majority of the 20 amino acid residue differences occurred in the CDR region of the molecules, a result of antibody engineering modifications for different antigen targets. On the basis of primary sequence and fixed pK_a values for amino acid side chains, the theoretical values of net charge at pH 6.0 on mAb1 (calcd pI 7.8) and mAb2 (calcd pI 9.2) are +17 and +30, respectively. Results from rheological studies suggest that primary sequence, net charge, and charge distribution differences are related to the self-association of mAb1 and are influenced by both salt concentration and salt type.[39] At low concentration, the average distance between macro-ions is large relative to molecular size, and the potential of electrostatic interaction between identical macro-ions is expected to be primarily due to (repulsive) monopole−monopole interactions. At high concentration, the average distance between macro-ions becomes comparable to the molecular size, and the electrostatic potential may be influenced by increased attractive interactions between localized charges of opposite sign. Here, SLS is used to investigate the intermolecular interactions that occur at concentrations ranging from 0.5 to 295 mg/mL of mAb1 and mAb2 as a function of salt concentration.

The measurements of light scattering from solutions of mAb1 and mAb2 were made with separate concentrations placed in individual vials. (For typical data, see Figure S-1 of the Supporting Information.) This permitted samples to be measured repeatedly and after equilibration with salt concentrations that ranged from 0 to 600 mM NaCl. In general, we observed that mAb2 solutions scattered less light than solutions of mAb1. Both sets of samples scattered light isotropically at the sample concentrations used (0−170 mg/mL mAb), indicating that no large irreversible aggregates were present or being formed. (See the representative data in Figure 1.) However, at the highest concentrations of mAb2 and mAb1 (295 and 225 mg/mL, respectively), nonlinear angular dependence of scattering intensity at the low angles was observed, as shown in Figure 1a, indicating that small amounts of irreversible high-molecular-weight aggregate species were present despite efforts to remove them by centrifugation. These aggregates most likely formed

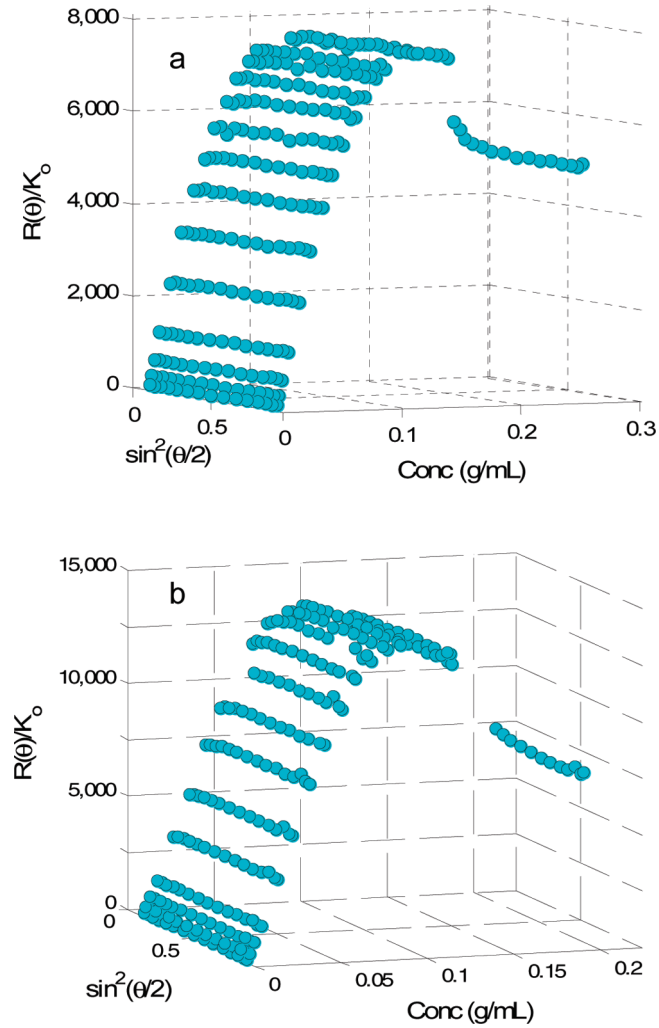

Figure 1. Light scattering intensity as a function of mAb concentration and scattering angle for representative experiments: (a) mAb2 in 30 mM buffer with 150 mM NaCl and (b) mAb1 in 30 mM buffer with 200 mM NaCl. The data generally show the isotropic scattering of each sample, with the highest concentration sample in part a showing angular dependency at the low-angle detectors. Outlier angle-dependent data were omitted from further analysis.

during the concentration process and may result from a gel-like concentrate layer observed on the membrane. Omitting the use of scattering data at angles below 50° (Figure 1b as an example) minimized the impact of such aggregates on the calculated M_{wApp} for these samples.

Scattering intensity ($R(\theta)/K_o$) measured at 90° for mAb2 as a function of mAb and NaCl concentration is shown in Figure 2a. The dependence of $R(\theta)/K_o$ on mAb concentration was clearly nonlinear. The Rayleigh ratios (scattered light intensity) obtained for mAb2 in pH 6.0, 10, and 30 mM histidine−HCl buffer alone were essentially independent of concentration above concentrations of 0.02 g/mL. With the addition of 20 to 150 mM NaCl to mAb2 solutions in 30 mM histidine−HCl, light scattering intensities were found to vary nonmonotonically across the entire antibody concentration range. Scattering intensities increased as a function of mAb2 concentration up to ~0.100 to ~0.125 g/mL, followed by decreases in scattering intensity at higher concentrations. Further ionic strength increases between 150 and 600 mM NaCl resulted in much smaller changes to scattering intensity profiles.

Experimentally measured concentration-dependent scattering can be compared with the calculated scattering for noninteracting

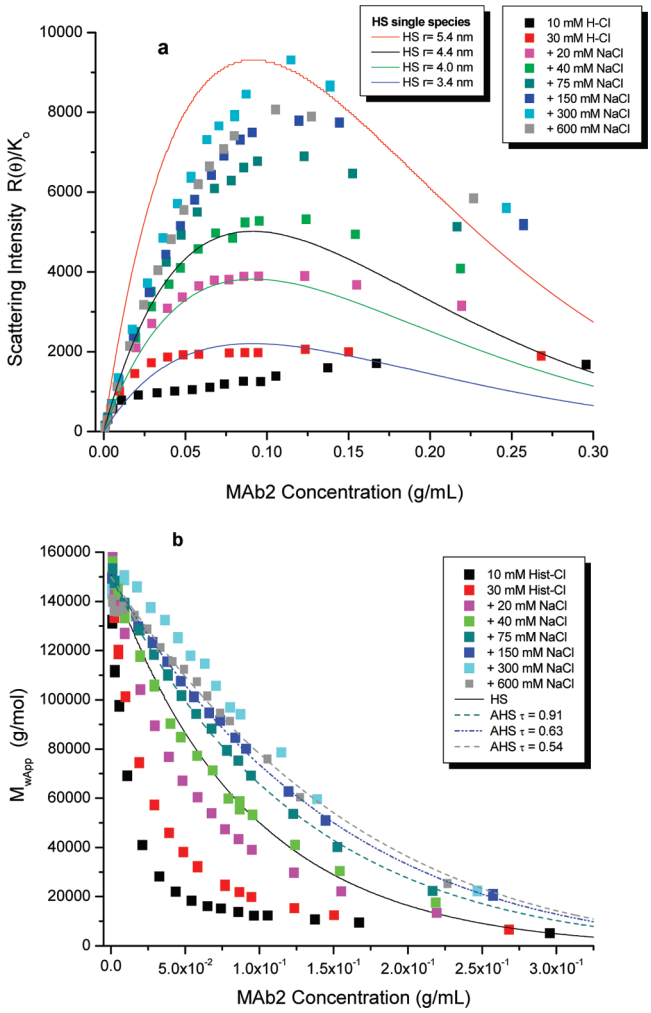

Figure 2. Light scattering as a function of mAb2 concentration presented in terms of scattering intensity from (a) $\theta = 90°$ and (b) apparent molecular weight M_{wApp}. The data obtained at different ionic strengths are represented as a series of colored data points, whereas HS and AHS models are shown as lines.

hard spheres, which describes the molecular excluded volume effects. A similar nonlinear concentration dependence of scattering intensity is also obtained for the calculated scattering for simple hard spheres with eqs 3−5, with calculated results for $r = 3.4$, 4.0, 4.4, and 5.4 nm shown in Figure 2a for comparison. Of these hard-sphere models, $r = 4.4$ nm provides an acceptable description of the data for mAb2 across the concentration range at 40 mM salt. When $r = 4.4$ nm (4.375 nm, to be exact, density = 0.71 g/mL), the P−Y hard-sphere scattering equation correctly returns the expected M of 150 kD for mAbs in the limit of infinite dilution. Fitting the 40 mM NaCl data set by all three models considered here yielded essentially identical values of the equivalent radius of mAb2 in the monodisperse hard-sphere limit. Finally, a spherical equivalent radius of ~4.4 nm (volume ~350 nm^3) for IgG is also obtained from scattering volumes determined by SAXS, which range from 265 to 400 nm^3 corresponding to $r = 4.0$ to 4.6 nm.[53−56] Therefore, for further comparisons, a value of $r = 4.4$ nm was used as a reasonable spherical approximation of IgG1 mAbs to determine volume fraction φ and hard-sphere light scattering.

Further evaluation of the scattering data for mAb2 is facilitated by plots of M_{wApp} versus concentration (Figure 2b) and by the use of osmotic compressibility plots (Figure S-2a of the Supporting Information), which at low concentrations provided A_2 values (summarized in Table S-1 of the Supporting Information) that ranged from (2.82 to 0.11) × 10^4 mol/(mL·g^2). In Figure 2b, M_{wApp} consistently decreases with increasing concentration, the extent of which was modulated by NaCl concentration or ionic strength. The M_{wApp} for a hard sphere of $r = 4.4$ nm calculated as a function of concentration bisects the salt dependence of the solution scattering data for mAb2. Solutions with 0−20 mM NaCl had lower M_{wApp} across the concentration range than the calculated HS scattering, considering only the excluded volume effect. In a solution of 30 mM buffer and 40 mM NaCl, mAb2 interactions across the concentration range are qualitatively well approximated by the HS model, where only the excluded volume contributed to the solution nonideality observed by light scattering. With the addition of 75−600 mM NaCl to mAb2 solutions, M_{wApp} values generally exceed those of the hard-sphere ($r = 4.4$ nm) model. When salt levels exceeded 40 mM, scattering data show that mAb2 interactions were less repulsive than predicted for hard spheres, suggesting a weakly attractive contribution to the total interaction potential (which includes steric repulsion) when electrostatic repulsions are screened. Simple comparison of light scattering data to the hard-sphere model provided plausible qualitative interpretation of the colloidal interactions present in mAb2 solutions. More quantitative interpretation could be obtained using the AHS model for a single species of interacting hard spheres and through the application of statistical-thermodynamic models incorporating multiple species of associating hard spheres.

Curve fitting analysis with the AHS model (eqs 6 and 7) using $r = 4.4$ nm, shown as broken lines in Figure 2b, resulted in good fits of scattering data for mAb2 in 40−150 and 600 mM NaCl. τ values decreased with increasing NaCl concentration, with $\tau = 1043$, 0.91, 0.63, and 0.54 for 40, 75, 150, and 600 mM NaCl, respectively. Resulting τ values had 95% confidence intervals smaller than ±0.01, with the exception of the 40 mM NaCl condition, where larger uncertainty resulted as the model limit of infinite τ was approached. τ is inversely proportional to attractive potential strength and in the AHS model of colloidal interactions is limited to short-range ($\leq 0.1*r$) intermolecular effects.[57] Small τ values of 0.23 to 0.1 influence calculated scattering intensity most, approaching the limits of strong adhesion.[19] τ values greater than 0.3 represent only weakly attractive deviations from the noninteracting HS model, which the AHS model reproduces when $\tau \geq 10^4$. The range of τ values (~1000−0.54) found for mAb2 concentration-dependent scattering as a function of NaCl concentration indicates the presence of weak, short-range attractive mAb−mAb interactions when solution ionic strength exceeded 40 mM NaCl.

The concentration dependence of light scattering in solutions of moderate ionic strength was also analyzed in detail using multicomponent scattering theory models for equilibrium self-association. Using this approach, we obtained a quantitative description of the scattering from mAb solutions containing at least 40 mM NaCl to provide estimates of the number, stoichiometry, and abundance of oligomeric species present as a function of total protein concentration. In Figure 3, the average measured scattering intensity $\langle R(\theta)\rangle/K_o$ is plotted as a function of mAb concentration (w_{tot}) for each solution of mAb2, in which NaCl ≥ 40 mM, together with the concentration-dependent scattering calculated, as described above using the best-fit parameter values shown in Table 1. According to this analysis, the scattering is accounted for by a simple reversible monomer−dimer self-association, with repulsive intermolecular interactions that vary little with salt concentration and attractive intermo-

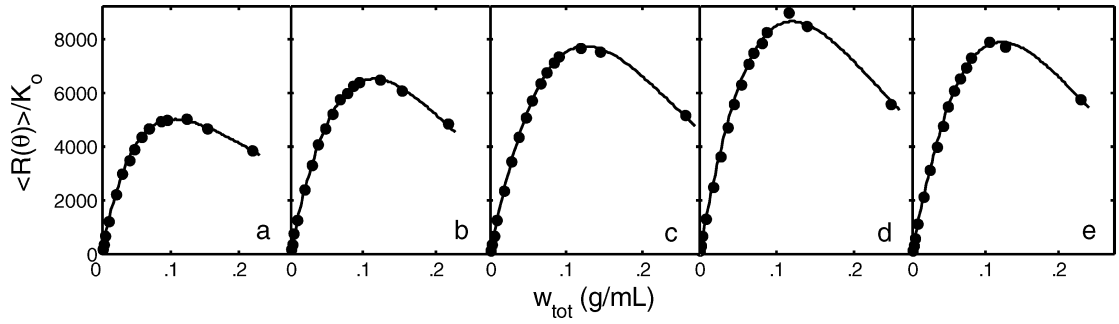

Figure 3. Concentration dependence of scattering intensity (data and calculated best fit of nonideal monomer−dimer model) for mAb2 in 30 mM histidine-Cl + (a) 40, (b) 75, (c) 150, (d) 300, and (e) 600 mM NaCl.

TABLE 1: Best Fit Parameters For mAb2 Data Modeled by a Monomer-Dimer Equilibrium Association Scheme with Solution Non-Ideality

	best fit parameter values		
NaCl (mM)	M_1	Log K_{12}°	v_{exc} (cm^3/g)
40	138 200	1.7	1.5
75		2.5	1.4
150		2.7	1.3
300		3.1	1.2
600		2.8	1.3

lecular interactions that increase modestly with increasing salinity before leveling off at the highest salt concentrations. It is important to note that even though the apparent weight-average molecular weight decreases monotonically with increasing total concentration at all NaCl levels, when contributions to the scattering intensity from excluded volume interactions are taken into account, reversible self-association becomes evident. With the reversible self-association of mAb2 to form dimeric species resolved, the actual weight-average molecular weight is seen to increase by as much as 80% at the highest antibody concentrations attained in the present study, as indicated in Figure S-3 of the Supporting Information.

Investigation of mAb1 SLS dependence on concentration and ionic strength provided a sharply contrasting example of thermodynamic solution behavior when compared with mAb2. Rayleigh ratios $R(\theta)/K_o$ measured as a concentration series for mAb1 in 30 mM histidine−HCl with 0−600 mM NaCl are shown in Figure 4a. mAb1 solutions scattered substantially more light than mAb2 samples under similar conditions. Several detector photodiodes saturated with excess scattering from samples at higher mAb1 concentrations and consequently $R(\theta)/K_o$ values in Figure 4a represent the data from $\theta = 141°$. After normalizing for the inherent differences in detector sensitivity, no significant angular dependency of the scattered light was observed, and results for M_{wApp} were obtained from linear extrapolation to $\theta = 0°$ using the remaining nonsaturating angles (including at least $\theta = 38$, 44, and 141°) for mAb1 samples. Calculated scattering intensities for hard spheres of several sizes ($r = 4.4-7.0$) are shown for comparison in terms of maximal scattering intensities in Figure 4a but clearly did not provide any acceptable fit to mAb1 scattering over the concentration range. In subsequent Figure 4b, only the HS scattering for $r = 4.4$ nm was used for comparison and interpretation.

In Figure 4b, apparent M_w measurements were distinctly nonlinear as a function of mAb1 concentration. Increases in M_{wApp} with concentration below ~0.050 g/mL clearly indicate that a degree of mAb1self-association occurred under most solution conditions examined. The magnitudes of net interactions initially determined from dilute solution behavior were evaluated in terms of the second virial coefficient, A_2. Negative A_2 values

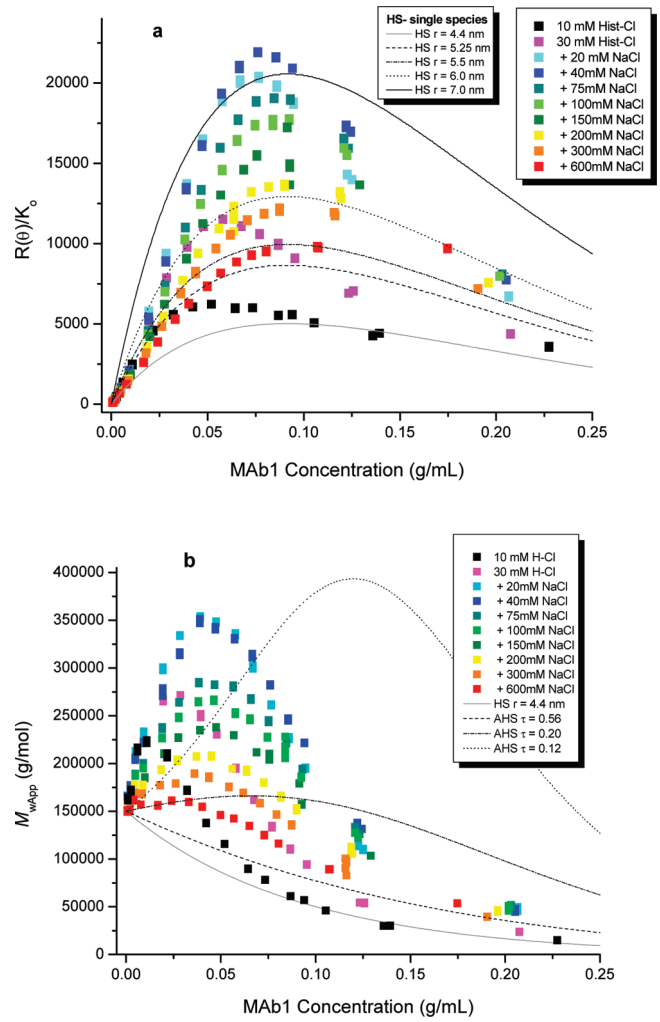

Figure 4. Light scattering as a function of mAb1 concentration presented in terms of scattering intensity from (a) $\theta = 141°$ and (b) apparent molecular weight M_{wApp}. The data obtained at different ionic strengths are represented as a series of data points, whereas HS and AHS models are shown as lines.

were obtained for all solutions of mAb1 and ranged from (−1.84 to −0.22) × 10^{-4} mol mL/g^2 (Table S-2 of the Supporting Information). Increases in NaCl concentration from 75 to 600 mM NaCl increased the A_2 magnitudes. Molecular weight values at infinite dilution (M) ranged from 156 to 162 kD, demonstrating that solutions of mAb1 existed as monomer species at infinite dilution, within the accuracy of the limited number concentrations ($n = 3$ to 4) used. Therefore, the increased M_{wApp} observed with increasing concentration reflects substantial reversible self-association of monomer species and attractive

intermolecular interactions. Values of M_{wApp} reached a maximum of 340−360 kDa in solutions with 30 mM histidine buffer and 20 mM NaCl between mAb1 concentrations of 0.035 and 0.05 g/mL. Above ∼50 mg/mL mAb1, apparent M_w decreased in nonlinear fashion for all solutions with increasing levels of NaCl. At the highest mAb concentrations of ∼0.200 g/mL, scattering M_{wApp} as well as osmotic compressibility (Figure S-2b of the Supporting Information) representations converged to values that changed little with varying solution conditions such as buffer and ionic strength. For mAb1 concentrations exceeding 0.050 g/mL, the decreasing M_{wApp} values in Figure 4b are indicative of the increasing contributions from repulsive interactions due to molecular crowding/excluded volume effects.

Apparent M_w across the mAb1 concentration range studied also showed a complex dependency on solution ionic strength (Figure 4b). To study the effects of ionic strength on mAb1 interactions, we prepared solutions with concentrations of 20−600 mM NaCl in 30 mM histidine buffer. Initial increases in the solution ionic strength up to 40 mM NaCl resulted in increased scattering and M_{wApp}. However, further increase in NaCl concentration from 75 to 600 mM NaCl decreased M_{wApp} across the concentrations tested. Comparison of mAb1 light scattering with that calculated with the noninteracting, single species HS model ($r = 4.4$ nm) provided an initial interpretation of the interactions of mAbs at high concentration. As is readily apparent, all solutions of mAb1 have substantially greater M_{wApp} values than for the noninteracting hard spheres. Added to pH 6.0 histidine buffer, increasing levels of NaCl incrementally decreased the scattering across the antibody concentrations. In general, we observed that increases in the ionic strength with NaCl reduced the strength of mAb1 attractive intermolecular interactions across the concentration range measured with SLS.

At first consideration, the salt dependence of mAb1 self-interactions determined here challenge established ideas about the colloidal nature of protein−protein interactions in low to moderate ionic strength conditions. In the classical DLVO model, proteins of identical net charge would be expected to have net repulsive electrostatic interactions that can be increasingly screened by the addition of salts, as seen in the case of mAb2. Although both the effect of NaCl and the attractive mAb1 interactions at low ionic strength do not fit this model of colloidal interactions, several observations made for other protein systems facilitate the interpretation of mAb1 solution behavior. Lesins et al.[58] found that protein surface adsorption may be controlled by the presence of localized opposite charge patches on proteins, despite net charge similarities. This localization or clustering of charged groups on the protein's surface has also been identified as a source of long-range electrostatic interactions, where two histidine residues on streptavidin switched the interactions with biotin from repulsive to attractive,[59,60] notably also at the pH 6.0 condition used here. Recently reported rheological characterization also determined that much of the propensity of mAb1 to self-associate is mediated by amino acid residues in the Fab domain, with multiple sites for interaction.[40] Other recent work demonstrated that molecular charge anisotropy may have a substantial role in protein−protein interactions and phase behavior.[61] These precedents, considered together with the decrease in attractive interactions as a function of NaCl observed by light scattering, support the conclusion that an anisotropic distribution of charge on mAb1 plays an important role in its self-association in solution. Furthermore, the role of NaCl in attenuating the interactions of mAb1 and mAb2 is essentially the same, as depicted in Figure 5, which shows the changes in A_2 as a function of the ionic strength. We conclude that NaCl screened Coulombic forces between mAbs regardless of whether the resulting interactions were net attractive or net repulsive (as commonly observed).

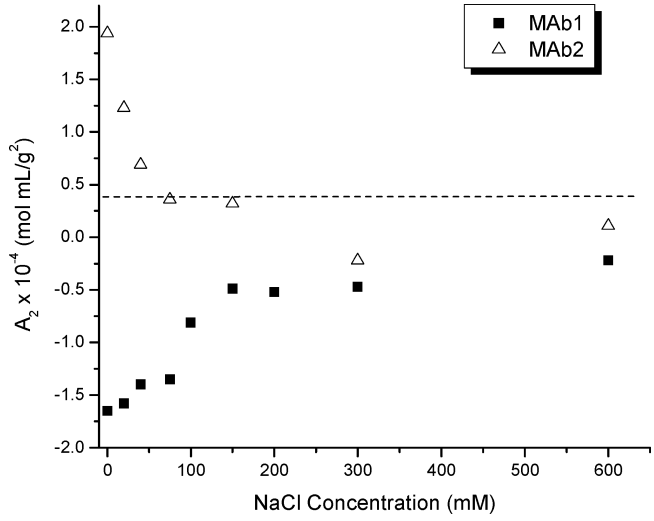

Figure 5. Osmotic second virial coefficients for mAb1 and mAb2 as a function of NaCl concentration. The dashed line represents the A_2 value of a hard sphere with $r = 4.4$ nm and $\upsilon_{exc} = 1.4$ cm^3/g.

Comparison of mAb1 scattering data with the predictions of the adhesive HS scattering model for different levels of τ (>1 to 0.1) indicated that this model was generally unsuccessful in fitting the scattering data obtained for mAb1 under any salt condition investigated. The theoretical concentration dependence calculated with $\tau = 0.15$ is shown in Figure 4b for comparison; this degree of adhesive interaction was only able to reproduce the maximum M_{wApp} obtained but was unable to describe the correct concentration dependence of mAb1 data. One potential reason for the failure of the Baxter AHS model to describe mAb1 scattering data is that the model is useful for describing effects of short-range interactions[57] but not longer-range attractive forces, as with electrostatic interactions. Another explanation may be that models based on a single HS species cannot account for the scattering of multiple species that results from significantly self-associating molecules.

In Figure 6, we apply the effective hard-sphere mixture model for up to three different species to simulate mAb1 data. The experimentally measured value of $<R(\theta)>/K_o$ is plotted as a function of w_{tot} for each solution of mAb1 in which [NaCl] ≥ 40 mM together with the concentration-dependent scattering calculated as described above using the best fit parameter values in Table 2. According to the best-fit model, the scattering is accounted for by reversible association of antibody to form equilibrium dimer and an equilibrium oligomer of stoichiometry $n = 4-6$ depending on salt concentrations. As pointed out elsewhere,[36] the ability of the three-species model to fit the data quantitatively does not necessarily indicate the presence of a single higher oligomer but could reflect a distribution of higher order oligomers centered about the best-fit value of n. The data do not provide information of sufficient resolution to distinguish between these possibilities. Nonetheless, the presence of a substantial mass fraction (>50%) of at least one oligomeric species of stoichiometry 4 or greater at the highest concentrations of mAb1 studied is required to account for the experimental data. When contributions to the scattering intensity from repulsive intermolecular interactions are taken into account, reversible self-association is seen to lead to an increase in actual weight-average molecular weight by a factor of between 3.5

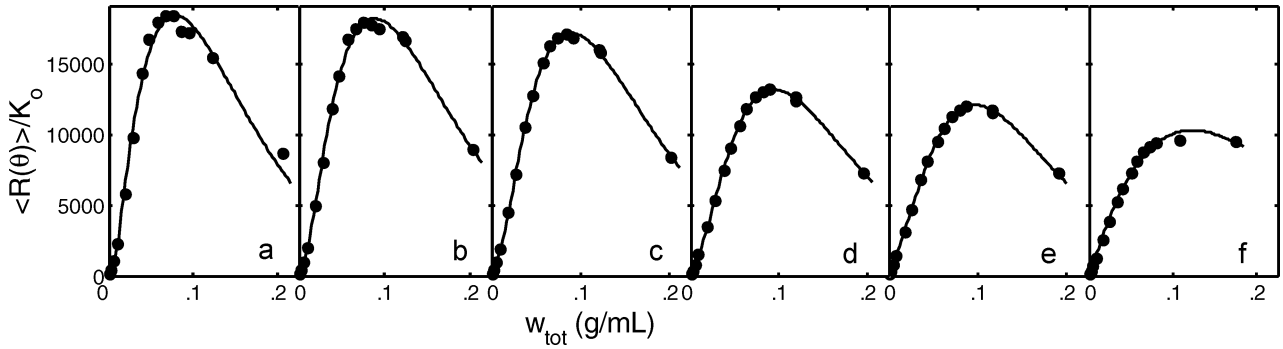

Figure 6. Concentration dependence of scattering intensity (data and calculated best fit of monomer−dimer-*n*-mer model) for mAb1 in 30 mM histidine-Cl + (a) 40, (b) 75, (c) 100, (d) 200, (e) 300, and (f) 600 mM NaCl.

TABLE 2: Best Fit Parameters for mAb1 Data Modeled by a Monomer−Dimer and Monomer−*n*-mer Equilibrium Association Scheme with Solution Non-Ideality

	best fit parameter values					
[NaCl]	M_1	m	Log $K_{1m}°$	n	Log $K_{1n}°$	v_{exc} (cm^3/g)
40	134 900	2	2.8(4.0)[a]	6	19.5(20.9)[a]	1.9
75			4.0		19.8	1.8
100			4.1		19.8	1.8
200			3.8	5	14.9	1.9
300			3.1		15.1	1.9
600			3.8	4	10.4	1.5

[a] Results from second least-squares fit with value of $K_{1m}°$ constrained to 4.0.

and 6 (depending upon salinity) at the highest antibody concentrations measured experimentally, as shown in Figure S-4 of the Supporting Information.

The effective specific exclusion volume v_{exc} appearing in the equivalent hard-sphere model is a measure of the magnitude of repulsive nonideal intermolecular interactions.[11,34] The extent to which this quantity exceeds the actual partial specific volume of the molecule (~0.73 cm^3/g) reflects multiple contributions arising from "soft" electrostatic repulsion, which is pH- and salt-dependent, protein solvation (hydration), and deviations of the shape of the molecule from an approximately spherical shape.[62] We note that in the case of mAb2 the best-fit value v_{exc} is approximately 1.4 ± 0.1 cm^3/g, roughly independent of salt concentration. Considering the simulation results for mAb2, it is evident that a specific volume of 1.5 cm^3/g and molar mass of 138.2 kD represent a spherically equivalent radius of 4.35 nm. This result is in excellent agreement with fitting results from the AHS models (R = 4.37 nm) and validates the assumption that an HS radius of 4.4 nm provides a good reference point against which the presence of interactions between IgG1 antibodies can be qualitatively assessed. In the case of mAb1, the best-fit value of v_{exc} is larger (~1.8 ± 0.1 cm^3/g) and is also insensitive to salt concentration, with the possible exception of the 600 mM NaCl solution. This effective volume and a mass of 134.9 kD yield a sphere equivalent radius of 4.6 nm for mAb1. The observation that effective volumes remain largely unaffected by salt concentration leads to the conclusion that the net repulsive interactions between both mAb 2 and mAb1 molecules at high concentration are dominated by steric rather than electrostatic interactions, and we speculate that the two different v_{exc} values may reflect different extents of deviation from a quasi-spherical conformation.

Conclusions

The self-interactions of two similar mAbs were investigated with SLS across a wide range of protein and salt concentrations to gain a greater understanding of the molecular interactions that contribute to high-concentration mAb solution properties. Measurement of mAb interactions at low concentration, quantified as A_2 showed that the interactions between molecules of mAb2 were net repulsive (positive A_2), whereas those between mAb1 molecules were net attractive (negative A_2). However, for the purpose of characterizing the concentration-dependent nonideal behavior, the second term of the osmotic virial expansion, A_2, is insufficient to describe the light scattering of proteins at high concentrations.

To interpret the complex solution nonideality at high concentrations, we compared SLS measurements of mAb1 and mAb2 with the scattering calculated for three different models based on equivalent hard spheres. In the limiting case of scattering from a single species of noninteracting hard spheres, all three models provided essentially the same result for the concentration-dependent scattering for mAb2 in 40 mM NaCl with a v_{eff} = 1.4 cm^3/g or r = 4.4 nm, although incorporating a small amount of self-association improved the fit of data above 100 g/L. Used as a reference point for the exclusion volume of IgG1 molecules, data comparison to this simple hard-sphere model permitted qualitative interpretation of the complex interactions observed above 10 g/L and could be applied equally well to low and high ionic strength solution conditions. With the use of the AHS model to interpret mAb solution nonideality, qualitative estimates of the strength and range of the intermolecular interactions may be made. Weak attractive interactions between IgG1 molecules were well-simulated by the AHS model, as calculated scattering profiles for mAb2 solutions with 40−600 mM NaCl show. However, the AHS model of interacting particles also fails when associative interactions are strong or longer range or when scattering contributions from multiple species are present as a function of concentration, as found for mAb1. In contrast, the effective hard-sphere mixture model of associating species was capable of describing mAb1 and mAb2 self-association due to both weak and strong nonspecific intermolecular attractive forces. It also provided quantitative estimates of oligomeric states, association constants, and repulsive interactions in the form of an effective molecular volume. This model permits analysis of the interactions of molecules across the entire range of concentrations studied, even in highly crowded systems where intermolecular interactions can be anticipated to be localized and influenced by multiple species and many-body interactions. In the overall analysis, the simulation of light scattering data with the simple hard-sphere and multispecies models of associating hard spheres were found to be consistent and complementary. All of the models account for excluded volume effects on light scattering data of IgG1 mAbs, but when allowance is made for additional features, such

as interactions in the AHS model and then mixtures of interacting scatterers, the quantitative description becomes more accurate.

The present Article demonstrates the utility of light scattering methods and different HS models for characterizing the self-association of proteins at high concentrations. Increasing solution ionic strength with NaCl was found to screen both net attractive and net repulsive interactions, indicating that electrostatic interactions as well as excluded volume effects play a significant role in both mAb1 and mAb2 solution behavior. Over the broad range of NaCl and protein concentrations, the data for mAb1 suggest that charge anisotropy or complementary patches of opposite charge can result in attractive electrostatic forces that contribute to protein association. Therefore, our observations also serve to underscore the complexity of nonspecific protein (colloidal) interactions and the need to better understand the solution thermodynamics of proteins at biotechnologically and physiologically relevant concentrations.

Acknowledgment. We would like to acknowledge insightful discussions with Daniel Some of Wyatt Technology Corporation as well as postdoctoral scientist Sonoko Kanai of Genentech, Inc. for her contributions. Research of APM is supported by the Intramural Research Program of the National Institute of Diabetes and Digestive and Kidney Diseases.

Supporting Information Available: Additional tables and figures cited in the text. This material is available free of charge via the Internet at http://pubs.acs.org.

References and Notes

(1) Bornhop, D. J.; Latham, J. C.; Kussrow, A.; Markov, D. A.; Jones, R. D.; Sorensen, H. S. *Science* **2007**, *317*, 1732.
(2) Berggård, T.; Linse, S.; James, P. *Proteomics* **2007**, *7*, 2833.
(3) Silverman, L.; Glick, D. *J. Cell Biol.* **1969**, *40*, 773.
(4) Adair, G. S. *Proc. R. Soc. London, Ser. A* **1928**, *120*, 573.
(5) Scatchard, G.; Batchelder, A. C.; Brown, A.; Zosa, M. *J. Am. Chem. Soc.* **1946**, *68*, 2610.
(6) Delaye, M.; Gromiec, A. *Biopolymers* **1983**, *22*, 1203.
(7) Vilker, V. L.; Colton, C. K.; Smith, K. A. *J. Colloid Interface Sci.* **1981**, *79*, 548.
(8) Williams, R. C. *Proc. Natl. Acad. Sci. U.S.A.* **1973**, *70*, 1506.
(9) Ross, P. D.; Briehl, R. W.; Minton, A. P. *Biopolymers* **1978**, *17*, 2285.
(10) Ross, P. D.; Minton, A. P. *J. Mol. Biol.* **1977**, *112*, 437.
(11) Minton, A. P.; Edelhoch, H. *Biopolymers* **1982**, *21*, 451.
(12) Andries, C.; Clauwaert, J. *Biophys. J.* **1985**, *47*, 591.
(13) Burz, D. S.; Dutta, K.; Cowburn, D.; Shekhtman, A. *Nat. Methods* **2006**, *3*, 91.
(14) Koenig, S. H.; Brown, R. D., III; Spiller, M.; Chakrabarti, B.; Pande, A. *Biophys. J.* **1992**, *61*, 776.
(15) Jimenez, M.; Rivas, G.; Minton, A. P. *Biochemistry* **2007**, *46*, 8373.
(16) Saluja, A.; Badkar, A. V.; Zeng, D. L.; Nema, S.; Kalonia, D. S. *Biophys. J.* **2007**, *92*, 234.
(17) Bonneté, F.; Malfois, M.; Finet, S.; Tardieu, S.; Lafont, S.; Veesler, S. *Acta Crystallogr., Sect. D: Biol. Crystallogr.* **1997**, *53*, 438.
(18) Chuan-Fu Wu, S.-H. C. *Biopolymers* **1988**, *27*, 1065.
(19) Fine, B. M.; Lomakin, A.; Ogun, O. O.; Benedek, G. B. *J. Chem. Phys.* **1996**, *104*, 326.
(20) Muschol, M.; Rosenberger, F. *J. Chem. Phys.* **1995**, *103*, 10424.
(21) Hall, D.; Minton, A. P. *Biochim. Biophys. Acta, Proteins Proteomics* **2003**, *1649*, 127.
(22) Baxter, R. J. *J. Chem. Phys.* **1968**, *49*, 2770.
(23) Leckband, D.; Sivasankar, S. *Colloids Surf., B* **1999**, *14*, 83.
(24) Rosenbaum, D. F.; Zukoski, C. F. *J. Cryst. Growth* **1996**, *169*, 752.
(25) Piazza, R. *J. Cryst. Growth* **1999**, *196*, 415.
(26) Jin, L.; Yu, Y.-X.; Gao, G.-H. *J. Colloid Interface Sci.* **2006**, *304*, 77.
(27) Pusey, P. N. Introduction to Scattering Experiments. In *Neutrons, X-rays and Light: Scattering Methods Applied to Condensed Soft Matter*; Lindner, P., Zemb, Th., Ed.; Elsevier: San Francisco, 2002.
(28) Tardieu, A.; Le Verge, A.; Malfois, M.; Bonneté, F.; Finet, S.; Riès-Kautt, M.; Belloni, L. *J. Cryst. Growth* **1999**, *196*, 193.
(29) Finet, S.; Skouri-Panet, F.; Casselyn, M.; Bonneté, F.; Tardieu, A. *Curr. Opin. Colloid Interface Sci.* **2004**, *9*, 112.
(30) Niebuhr, M.; Koch, M. H. J. *Biophys. J.* **2005**, *89*, 1978.
(31) Krueger, S.; Chen, S. H.; Hofrichter, J.; Nossal, R. *Biophys. J.* **1990**, *58*, 745.
(32) Wu, C.-F.; Chen, S.-H. *J. Chem. Phys.* **1987**, *87*, 6199.
(33) Zhang, F.; Skoda, M. W. A.; Jacobs, R. M. J.; Martin, R. A.; Martin, C. M.; Schreiber, F. *J. Chem. Phys. B* **2007**, *111*, 251.
(34) Minton, A. P. *J. Pharm. Sci.* **2007**, *96*, 3466.
(35) Xia, J. Z.; Wang, Q.; Tatarkova, S.; Aerts, T.; Clauwaert, J. *Biophys. J.* **1996**, *71*, 2815.
(36) Fernandez, C.; Minton, A. P. *Biophys. J.* **2009**, *96*, 1992.
(37) Hall, D.; Minton, A. P. *Biochim. Biophys. Acta* **2003**, *1649*, 127.
(38) Liu, Y.; Fratini, E.; Baglioni, P.; Chen, W.-R.; Chen, S.-H. *Phys. Rev. Lett.* **2005**, *95*, 118102.
(39) Liu, J.; Nguyen, M. D.; Andya, J. D.; Shire, S. J. *J. Pharm. Sci.* **2005**, *94*, 1928.
(40) Kanai, S.; Liu, J.; Patapoff, T. W.; Shire, S. J. *J. Pharm. Sci.* **2008**, *97*, 4219.
(41) Yadav, S.; Liu, J.; Shire, S. J.; Kalonia, D. S. *J. Pharm. Sci.* **2010**, 99, 1152.
(42) Vrij, A.; Jansen, J. W.; Dhont, J. K. G.; Pathmamanoharan, C.; Kops-Werkhoven, M. M.; Fijnaut, H. M. *Faraday Discuss. Chem. Soc.* **1983**, *76*, 19.
(43) Tanford, C. *The Physical Chemistry of Macromolecules*; John Wiley and Sons: New York, 1961.
(44) Kerker, M. Scattering by Liquids. In *The Scattering of Light and Other Electromagnetic Radiation*; Kerker, M., Ed.; Academic Press: New York, 1969; p 573.
(45) Bettelheim, F. A.; Siew, E. L. *Biophys. J.* **1983**, *41*, 29.
(46) Theisen, A.; Johann, C.; Deacon, M. P.; Harding, S. E. *Refractive Increment Data-Book for Polymer and Biomolecular Scientists*; Nottingham University Press: Nottingham, U.K., 2000.
(47) Mochrie, S. Boulder Summer School 2006; The Percus-Yevick equation, http://xpcs.physics.yale.edu/boulder1/node30.html, (07-14-2006).
(48) Barboy, B. *J. Chem. Phys.* **1974**, *61*, 3194.
(49) Stockmayer, W. H. *J. Chem. Phys.* **1950**, *18*, 58.
(50) Kirkwood, J. G.; Goldberg, R. J. *J. Chem. Phys.* **1950**, *18*, 54.
(51) Minton, A. P. *Biophys. J.* **2007**, *93*, 1321.
(52) Lebowitz, J. L.; Helfand, E.; Praestgaard, E. *J. Chem. Phys.* **1965**, *43*, 774.
(53) Pilz, I.; Kratky, O.; Karush, F. *Eur. J. Biochem.* **1974**, *41*, 91.
(54) Pilz, I.; Kratky, O.; Licht, A.; Sela, M. *Biochemistry* **1973**, *12*, 4998.
(55) Pilz, I.; Schwarz, E.; Palm, W. *Eur. J. Biochem.* **1977**, *75*, 195.
(56) Volkov, V. V.; Lapuk, V. A.; Kayushina, R. L.; Shtykova, E. V.; Varlamova, E. Yu.; Malfois, M.; Svergun, D. I. *J. Appl. Crystallogr.* **2003**, *36*, 503.
(57) Regnaut, C.; Ravey, J. C. *J. Chem. Phys.* **1989**, *91*, 1211.
(58) Lesins, V.; Ruckenstein, E. *Colloid Polym. Sci.* **1988**, *266*, 1187.
(59) Leckband, D. E.; Schmitt, F. J.; Israelachvili, J. N.; Knoll, W. *Biochemistry* **1994**, *33*, 4611.
(60) Sivasankar, S.; Subramaniam, S.; Leckband, D. *Proc. Natl. Acad. Sci. U.S.A.* **1998**, *95*, 12961.
(61) McManus, J. J.; Lomakin, A.; Ogun, O.; Pande, A.; Basan, M.; Pande, J.; Benedek, G. B. *Proc. Natl. Acad. Sci. U.S.A.* **2007**, *104*, 16856.
(62) Minton, A. P. *Curr. Opin. Biotechnol.* **1997**, *8*, 65.

JP1028646